THE INTEGRAL EQUATION APPROACH TO KINEMATIC DYNAMO THEORY AND ITS APPLICATION TO DYNAMO EXPERIMENTS IN CYLINDRICAL GEOMETRY

M. Xu[1], F. Stefani[*], G. Gerbeth

Forschungszentrum Dresden-Rossendorf, P.O. Box 510119, D-01314 Dresden, Germany

Abstract

The conventional magnetic induction equation that governs hydromagnetic dynamo action is transformed into an equivalent integral equation system. An advantage of this approach is that the computational domain is restricted to the region occupied by the electrically conducting fluid and to its boundary. This integral equation approach is first employed to simulate kinematic dynamos excited by Beltrami-like flows in a finite cylinder. The impact of externally added layers around the cylinder on the onset of dynamo actions is investigated. Then it is applied to simulate dynamo experiments within cylindrical geometry including the "von Kármán sodium" (VKS) experiment and the Riga dynamo experiment. A modified version of this approach is utilized to investigate magnetic induction effects under the influence of externally applied magnetic fields which is also important to measure the proximity of a given dynamo facility to the self-excitation threshold.

Key words: Magnetohydrodynamics, Dynamo, Integral equation

[*] Corresponding author. Tel.: +49 351 260 3069: fax: +49 351 260 2007.
 Email address: F.Stefani@fzd.de (F. Stefani).
[1] Present address: Center for Space Thermal Science, Shandong University, P.O.Box 88, Jin Shi Road 73, Jinan City, Shandong Province, P. R. China

1 INTRODUCTION

Dynamo action in moving electrically conducting fluids explains the existence
of cosmic magnetic fields, including the fields of planets, stars, and galaxies [1].
As long as the magnetic field is weak and its influence on the velocity field is
negligible we speak about the *kinematic dynamo regime*. When the magnetic
field has gained higher amplitudes the velocity field will be modified, and the
dynamo enters its saturation regime.

The usual way to simulate dynamos numerically is based on the induction
equation for the magnetic field $\mathbf{B}$,

$$\frac{\partial \mathbf{B}}{\partial t} = \nabla \times (\mathbf{u} \times \mathbf{B}) + \frac{1}{\mu\sigma}\Delta\mathbf{B}, \quad \nabla \cdot \mathbf{B} = 0, \tag{1}$$

where $\mathbf{u}$ is the given velocity field, μ the permeability of the fluid, and σ its
electrical conductivity. The behaviour of the magnetic field $\mathbf{B}$ in Eq. (1) is
controlled by the ratio of field production and field dissipation, expressed by
the magnetic Reynolds number $R_m = \mu\sigma LU$, where L and U are typical length
and velocity scales of the flow, respectively. When the magnetic Reynolds
number reaches a critical value, henceforth denoted by R_m^c, the dynamo starts
to operate.

Equation (1) follows directly from pre-Maxwell's equations and Ohm's law in
moving conductors. In order to make this equation solvable, boundary con-
ditions of the magnetic field must be prescribed. In the case of vanishing
excitations of the magnetic field from outside the considered finite region, the
boundary condition of the magnetic field is given as follows:

$$\mathbf{B} = O(r^{-3}) \text{ as } r \to \infty. \tag{2}$$

Kinematic dynamos are usually simulated in the framework of the differential
equation approach by solving the induction equation (1). For spherical dy-
namos, as they occur in planets and stars, the problem of implementing the
non-local boundary conditions for the magnetic field is easily solved by using
decoupled boundary conditions for each degree of the spherical harmonics. For
other than spherically shaped dynamos, in particular for galactic dynamos and
some of the recent laboratory dynamos working in cylindrical geometry [2],
the handling of the non-local boundary conditions is a notorious problem.

The simplest way to circumvent this problem is to replace the non-local bound-
ary conditions by simplified local ones (so-called vertical field condition). This
is often used in the simulation of galactic dynamos [3], and has also been
tested in an approximate simulation of the Riga dynamo experiment [4].

For the simulation of the cylindrical Karlsruhe dynamo experiment, the actual electrically conducting region was embedded into a sphere, and the region between the sphere and the surface of the dynamo was virtually filled by a medium of lower electrical conductivity [5,6].

Of course, both methods are connected with losses of accuracy. In order to fully implement the nonlocal boundary condition, Maxwell's equations must be fulfilled in the exterior, too. This can be implemented in different ways. For the finite difference simulation of the Riga dynamo, the Laplace equation was solved (for each time-step) in the exteriour of the dynamo domain and the magnetic field solutions in the interiour and in the exteriour were matched using interface conditions [7]. A similar method, although based on the finite element method, was presented by Guermond et al. [8,9]. Another, and quite elegant, technique to circumvent the solution in the exteriour was presented by Iskakov et al. [10,11] where a combination of a finite volume and a boundary element method was used to circumvent the discretization of the outer domain.

An alternative to the differential equation approach (DEA) based on the solution of the induction equation is the integral equation approach (IEA) for kinematic dynamos which basically relies on the self-consistent treatment of Biot-Savart's law. For the case of a steady dynamo acting in infinite domains of homogeneous conductivity, the integral equation approach had already been employed by a few authors [12,13,14,15]. For the case of finite domains, the simple Biot-Savart equation has to be supplemented by a boundary integral equation for the electric potential [16,17]. If the magnetic field becomes time-dependent, yet another equation for the magnetic vector potential has to be added [18].

In the present work, the integral equation approach is applied to various dynamo problems in cylindrical geometry. Two variants of the approach are presented: in the first one, it is implemented as an eigenvalue solver to solve genuine dynamo problems. In the second one, it is used to treat induction effects in the case of externally applied magnetic fields. Actually, the first variant was already at the root of the paper [19] where a surprising negative impact of sodium layers behind the propellers in the "von Kármán sodium" (VKS) experiment was identified. It was not least this finding that prompted the VKS team to modify the experiment which made it ultimately succesful [20,21]. After the derivation of the equation system in cylindrical geometry, we switch over to the treatment of specific problems, including the free decay case, the mentioned "von Kármán sodium" (VKS) experiment [22,23], and the Riga dynamo experiment [24,25,26].

2 MATHEMATICAL FORMULATION

Assume the electrically conducting fluid be confined in a finite region V with boundary S, the exterior of this region filled by insulating material or vacuum. Then, dynamo and induction processes can be described [16] by the following integral equation system:

$$\mathbf{b}(\mathbf{r}) = \frac{\mu\sigma}{4\pi} \int\limits_V \frac{(\mathbf{u}(\mathbf{r}') \times (\mathbf{B}_0(\mathbf{r}') + \mathbf{b}(\mathbf{r}'))) \times (\mathbf{r} - \mathbf{r}')}{|\mathbf{r} - \mathbf{r}'|^3} dV'$$

$$-\frac{\mu\sigma\lambda}{4\pi} \int\limits_V \frac{\mathbf{A}(\mathbf{r}') \times (\mathbf{r} - \mathbf{r}')}{|\mathbf{r} - \mathbf{r}'|^3} dV' - \frac{\mu\sigma}{4\pi} \int\limits_S \phi(\mathbf{s}')\mathbf{n}(\mathbf{s}') \times \frac{\mathbf{r} - \mathbf{s}'}{|\mathbf{r} - \mathbf{s}'|^3} dS' \quad (3)$$

$$\frac{1}{2}\phi(\mathbf{s}) = \frac{1}{4\pi} \int\limits_V \frac{(\mathbf{u}(\mathbf{r}') \times (\mathbf{B}_0(\mathbf{r}') + \mathbf{b}(\mathbf{r}'))) \cdot (\mathbf{s} - \mathbf{r}')}{|\mathbf{s} - \mathbf{r}'|^3} dV'$$

$$-\frac{\lambda}{4\pi} \int\limits_V \frac{\mathbf{A}(\mathbf{r}') \cdot (\mathbf{s} - \mathbf{r}')}{|\mathbf{s} - \mathbf{r}'|^3} dV' - \frac{1}{4\pi} \int\limits_S \phi(\mathbf{s}')\mathbf{n}(\mathbf{s}') \cdot \frac{\mathbf{s} - \mathbf{s}'}{|\mathbf{s} - \mathbf{s}'|^3} dS' \quad (4)$$

$$\mathbf{A}(\mathbf{r}) = \frac{1}{4\pi} \int\limits_V \frac{(\mathbf{B}_0(\mathbf{r}') + \mathbf{b}(\mathbf{r}')) \times (\mathbf{r} - \mathbf{r}')}{|\mathbf{r} - \mathbf{r}'|^3} dV'$$

$$+\frac{1}{4\pi} \int\limits_S \mathbf{n}(\mathbf{s}') \times \frac{\mathbf{B}_0(\mathbf{s}') + \mathbf{b}(\mathbf{s}')}{|\mathbf{r} - \mathbf{s}'|} dS', \quad (5)$$

where $\mathbf{B}_0$ is the externally applied magnetic field (which might be zero), $\mathbf{b}$ the induced magnetic field, $\mathbf{u}$ the velocity field, μ the permeability of the fluid (which is in most relevant cases the permeability of the vacuum), σ the electrical conductivity, $\mathbf{A}$ the vector potential, and ϕ the electric potential. $\mathbf{n}$ denotes the outward directed unit vector at the boundary S. For a steady velocity field, the time dependence of all electromagnetic fields can be assumed to be $\sim \exp \lambda t$. We have to distinguish three different cases: For non-zero $\mathbf{B}_0$, and below the self-excitation threshold, the imaginary part of λ is simply the angular frequency of the applied and also of the induced magnetic field. For $\mathbf{B}_0 = 0$ the equation system (3-5) represents an eigenvalue equation for the unknown time constant λ whose real part is the growth rate, and its imaginary part the angular frequency of the fields. For $\mathbf{B}_0 = 0$ and $\lambda = 0$, we need only the equations (3) and (4) which then represent an eigenvalue problem for the critical value of the velocity $\mathbf{u}$ at which the (non-oscillatory) dynamo starts to work.

2.1 General numerical scheme

Although, in this paper, we will focus mainly on cylindrical systems it might be instructive to delineate the general numerical scheme for the solution of Eqs. (3-5).

Assuming a specific discretization of all fields in Eqs. (3-5), we obtain

$$b_i = \mu\sigma[P_{ik}(B_{0k} + b_k) - \lambda R_{ij}A_j - Q_{il}\phi_l], \tag{6}$$
$$G_{ml}\phi_l = S_{mk}(B_{0k} + b_k) - \lambda T_{mj}A_j, \tag{7}$$
$$A_j = W_{jk}(B_{0k} + b_k), \tag{8}$$

where Einstein's summation convention is assumed. We have used the notion $G_{ml} = 0.5\,\delta_{ml} + U_{ml}$. B_{0k} and b_k denote the degrees of freedom of the externally added magnetic field and the induced magnetic field, A_j the degrees of freedom of the vector potential in the volume V, ϕ_l the degrees of freedom of the electric potential at the boundary surface. Note that only the matrices P_{ik} and S_{mk} depend on the velocity (the sources of the dynamo action), while R_{ij}, Q_{il}, T_{mj}, G_{ml} and W_{jk} depend only on the geometry of the dynamo domain and the discretization details.

Substituting Eqs.(7) and (8) into Eq.(6) and eliminating A_j and ϕ_l gives one single matrix equation for the induced magnetic field components b_i:

$$b_i = \mu\sigma[P_{ik}(B_{0k} + b_k) - \lambda R_{ij}W_{jk}(B_{0k} + b_k) - Q_{il}G_{lm}^{-1}S_{mk}(B_{0k} + b_k)$$
$$+ \lambda Q_{il}G_{lm}^{-1}T_{mj}W_{jk}(B_{0k} + b_k)]. \tag{9}$$

This equation can be further rewritten in the following form:

$$[\delta_{ik} - \mu\sigma E_{ik} - \mu\sigma\lambda F_{ik}]b_k = [\mu\sigma E_{ik} + \mu\sigma\lambda F_{ik}]B_{0k}, \tag{10}$$

where $E_{ik} = P_{ik} - Q_{il}G_{im}^{-1}S_{mk}$ and $F_{ik} = -R_{ij}W_{jk} + Q_{il}G_{lm}^{-1}T_{mj}W_{jk}$. To compute induction effects, the induced magnetic field is obtained by solving the algebraic equation system (10). For the kinematic dynamo, Eq.(10) reduces to the following generalized eigenvalue problem

$$[\delta_{ik} + \mu\sigma E_{ik}]b_k = \lambda^* F_{ik}b_k, \tag{11}$$

where λ^* is a new time constant rescaled according to $\lambda^* = \mu\sigma\lambda$.

2.2 Cylindrical Geometry

Since a number of dynamo experiments are carried out in cylindrical vessels, it is worth to specify the integral equation approach to this geometry. As long as the dynamo source (i.e. the velocity field or a corresponding mean-field quantity) is axisymmetric, the different azimuthal modes of the electromagnetic fields can be decoupled. This leads to a tremendous reduction of the numerical effort. The price we have to pay for this is the necessity to carefully deriving the dimensionally reduced version of the integral equation system.

The electrically conducting fluid is assumed to be confined in a cylinder with radius R and height $2H$. Introducing the cylindrical coordinate system (ρ, φ, z), we have

$$\mathbf{r} = [\rho \cos \varphi, \rho \sin \varphi, z]^T, \mathbf{b} = [b_\rho, b_\varphi, b_z]^T, \mathbf{u} = [u_\rho, u_\varphi, u_z]^T. \tag{12}$$

The magnetic field $\mathbf{b}$, the electric potential ϕ, and the vector potential $\mathbf{A}$ are expanded into azimuthal modes:

$$\begin{pmatrix} \mathbf{b} \\ \phi \\ \mathbf{A} \end{pmatrix} = \sum_{m=-\infty}^{\infty} \begin{pmatrix} \mathbf{b}_m \\ \phi_m \\ \mathbf{A}_m \end{pmatrix} \exp(im\varphi). \tag{13}$$

When the velocity field is axisymmetric (i.e. it has only a component with $m = 0$), one can see that $[\mathbf{b}_m, \phi_m, \mathbf{A}_m]^T (m = 0, \pm 1, \pm 2, \cdots)$ are decoupled with respect to m and they only depend on the variables (ρ, z). Henceforth, we always re-denote $[\mathbf{b}_m, \phi_m, \mathbf{A}_m]^T$ as $[\mathbf{b}, \phi, \mathbf{A}]^T$ for abbreviation. Then, after integrating over φ, Eq.(3) acquires the form

$$\begin{aligned}
b_\rho = \frac{\mu\sigma}{4\pi} [&\int_{-H}^{H} \int_{0}^{R} [((z - z')E_c^m u_z - i\rho' E_s^m u_\varphi)(B_{0\rho} + b_\rho) + (-i(z - z')u_z E_s^m \\
&+ i\rho' E_s^m u_\rho)(B_{0\varphi} + b_\varphi) + (i(z - z')E_s^m u_\varphi - (z - z')u_\rho E_c^m)(B_{0z} + b_z)]\rho' d\rho' dz' \\
&- \int_{0}^{R} \phi \rho'^2 E_s^m |_{z'=H} d\rho' - \int_{-H}^{H} \phi R(z - z')E_s^m |_{\rho'=R} dz' + \int_{0}^{R} \phi \rho'^2 E_s^m |_{z'=-H} d\rho' \\
&- \lambda \int_{-H}^{H} \int_{0}^{R} ((z - z')E_s^m A_\rho + (z - z')E_c^m A_\varphi + \rho' E_s^m A_z)\rho' d\rho' dz'], \tag{14}
\end{aligned}$$

$$\begin{aligned}
b_\varphi = \frac{\mu\sigma}{4\pi} [&\int_{-H}^{H} \int_{0}^{R} [(-(\rho E_1^m - \rho' E_c^m)u_\varphi + i(z - z')u_z E_s^m)(B_{0\rho} + b_\rho) \\
&+ ((\rho E_1^m - \rho' E_c^m)u_\rho + (z - z')u_z E_c^m)(B_{0\varphi} + b_\varphi) + (-(z - z')u_\varphi E_c^m
\end{aligned}$$

$$-i(z-z')u_\rho E_s^m)(B_{0z}+b_z)]\rho'd\rho'dz' - \int_0^R \phi(\rho\rho' E_1^m|_{z'=H} - \rho'^2 E_c^m|_{z'=H})d\rho'$$

$$+\int_{-H}^H \phi R(z-z')E_c^m|_{\rho'=R}dz' - \int_0^R \phi(-\rho E_1^m|_{z'=-H} + \rho' E_c^m|_{z'=-H})\rho'd\rho'$$

$$-\lambda\int_{-H}^H\int_0^R ((z-z')E_s^m A_\varphi - (z-z')E_c^m A_\rho + (\rho E_1^m - \rho' E_c^m)A_z)\rho'd\rho'dz'], \quad (15)$$

$$b_z = \frac{\mu\sigma}{4\pi}[\int_{-H}^H\int_0^R [(\rho' E_1^m - \rho E_c^m)u_z(B_{0\rho}+b_\rho) + i\rho E_s^m u_z(B_{0\varphi}+b_\varphi)$$

$$+((-\rho' E_1^m + \rho E_c^m)u_\rho - i\rho E_s^m u_\varphi)(B_{0z}+b_z)]\rho'd\rho'dz' + \int_{-H}^H \phi R\rho E_s^m|_{\rho'=R}dz'$$

$$-\lambda\int_{-H}^H\int_0^R(-\rho E_s^m A_\rho + (\rho' E_1^m - \rho E_c^m)A_\varphi)\rho'd\rho'dz'], \quad (16)$$

where the following azimuthal integrals appear:

$$E_1^m(\rho,\rho',z,z') = \int_0^{2\pi} \frac{\cos m\varphi'}{(\rho^2 + \rho'^2 - 2\rho\rho'\cos\varphi' + (z-z')^2)^{\frac{3}{2}}}d\varphi',$$

$$E_c^m(\rho,\rho',z,z') = \int_0^{2\pi} \frac{\cos m\varphi'\cos\varphi'}{(\rho^2 + \rho'^2 - 2\rho\rho'\cos\varphi' + (z-z')^2)^{\frac{3}{2}}}d\varphi',$$

$$E_s^m(\rho,\rho',z,z') = \int_0^{2\pi} \frac{\sin m\varphi'\sin\varphi'}{(\rho^2 + \rho'^2 - 2\rho\rho'\cos\varphi' + (z-z')^2)^{\frac{3}{2}}}d\varphi'.$$

Accordingly, from Eq.(4), we obtain the expressions for the electric potentials at the three different surface parts of the cylinder:

$$\frac{1}{2}\phi(s_1) = \frac{1}{4\pi}[\int_{-H}^H\int_0^R(-\rho'\rho E_s^m|_{z=H}u_z - \rho'(H-z')u_\varphi E_1^m|_{z=H})(B_{0\rho}+b_\rho)$$

$$+((-\rho'\rho E_c^m|_{z=H} + \rho'^2 E_1^m|_{z=H})u_z + \rho'(H-z')u_\rho E_1^m|_{z=H})(B_{0\varphi}+b_\varphi)$$

$$+((\rho'\rho E_c^m|_{z=H} - \rho'^2 E_1^m|_{z=H})u_\varphi + \rho'\rho E_s^m|_{z=H}u_\rho)(B_{0z}+b_\varphi)d\rho'dz'$$

$$-\int_{-H}^H \phi R(\rho E_c^m|_{\rho'=R,z=H} - RE_1^m|_{\rho'=R,z=H})dz'$$

$$+2.0H\int_0^R \phi E_1^m|_{z=H,z'=-H}\rho'd\rho' - \lambda\int_{-H}^H\int_0^R \rho'(\rho E_c^m|_{z=H} - \rho' E_1^m|_{z=H})A_\rho$$

$$-\rho'\rho E_s^m|_{z=H}A_\varphi + \rho'(H-z')E_1^m|_{z=H}A_z d\rho' dz'], \tag{17}$$

$$\frac{1}{2}\phi(s_2) = \frac{1}{4\pi}[\int\limits_{-H}^{H}\int\limits_{0}^{R}(-\rho' R E_s^m|_{\rho=R}u_z - \rho'(z-z')u_\varphi E_1^m|_{\rho=R})(B_{0\rho}+b_\rho)$$

$$+(-\rho' R E_c^m|_{\rho=R}u_z + \rho'^2 E_1^m|_{\rho=R}u_z + \rho'(z-z')u_\rho E_1^m|_{\rho=R})(B_{0\varphi}+b_\varphi)$$

$$+(\rho' u_\varphi R E_c^m|_{\rho=R} + \rho' R u_\rho E_s^m|_{\rho=R} - \rho'^2 u_\varphi E_1^m|_{\rho=R})(B_{0z}+b_z)d\rho' dz'$$

$$-\int\limits_{0}^{R}\phi(z-H)E_1^m|_{\rho=R,z'=H}\rho' d\rho' - \int\limits_{-H}^{H}\phi(E_c^m|_{\rho=\rho'=R} - E_1^m|_{\rho=\rho'=R})R^2 dz'$$

$$+\int\limits_{0}^{R}\phi(z+H)E_1^m|_{\rho=R,z'=-H}\rho' d\rho' - \lambda\int\limits_{-H}^{H}\int\limits_{0}^{R}(\rho' R E_c^m|_{\rho=R}$$

$$-\rho'^2 E_1^m|_{\rho=R})A_\rho - \rho' R E_s^m|_{\rho=R}A_\varphi + \rho'(z-z')E_1^m|_{\rho=R}A_z d\rho' dz'], \tag{18}$$

$$\frac{1}{2}\phi(s_3) = \frac{1}{4\pi}[\int\limits_{-H}^{H}\int\limits_{0}^{R}(-\rho'\rho E_s^m|_{z=-H}u_z + \rho'(H+z')E_1^m|_{z=-H}u_\varphi)(B_{0\rho}+b_\rho)$$

$$+(-\rho'\rho E_c^m|_{z=-H}u_z + \rho'^2 E_1^m|_{z=-H}u_z - \rho'(H+z')u_\rho E_1^m|_{z=-H})(B_{0\varphi}+b_\varphi)$$

$$+(\rho'\rho u_\varphi E_c^m|_{z=-H} - \rho'^2 u_\varphi E_1^m|_{z=-H} + \rho'\rho u_\rho E_s^m|_{z=-H})(B_{0z}+b_z)d\rho' dz'$$

$$+2.0H\int\limits_{0}^{R}\phi E_1^m|_{z=-H,z'=H}\rho' d\rho' - \int\limits_{-H}^{H}\phi R(\rho E_c^m|_{\rho'=R,z=-H}$$

$$-R E_1^m|_{\rho'=R,z=-H})dz' - \lambda\int\limits_{V}(\rho\rho' E_c^m|_{z=-H} - \rho'^2 E_1^m|_{z=-H})A_\rho$$

$$-\rho'\rho E_s^m|_{z=-H}A_\varphi + \rho'(-H-z')A_z E_1^m|_{z=-H}d\rho' dz']. \tag{19}$$

Here, s_1 is the surface $z = H$, s_2 the surface $\rho = R$, s_3 the surface $z = -H$. Equation (5) for the vector potential gets the form

$$A_\rho = \frac{1}{4\pi}[\int\limits_{-H}^{H}\int\limits_{0}^{R}\rho'(z-z')E_s^m(B_{0\rho}+b_\rho) + \rho'(z-z')E_c^m(B_{0\varphi}+b_\varphi)$$

$$+\rho'^2 E_s^m(B_{0z}+b_z)d\rho' dz' + \int\limits_{0}^{R}-\rho' D_s^m|_{z'=H}(B_{0\rho}+b_\rho) - \rho' D_c^m|_{z'=H}(B_{0\varphi}+b_\varphi)d\rho'$$

$$+\int\limits_{-H}^{H}R(B_{0z}+b_z)D_s^m|_{\rho'=R}dz' + \int\limits_{0}^{R}\rho' D_s^m|_{z'=-H}(B_{0\rho}+b_\rho)$$

$$+\rho'(B_{0\varphi}+b_\varphi)D_c^m|_{z'=-H}d\rho'] \tag{20}$$

$$A_\varphi = \frac{1}{4\pi}[\int\limits_{-H}^{H}\int\limits_{0}^{R}-\rho'(z-z')E_c^m(B_{0\rho}+b_\rho) + \rho'(z-z')E_s^m(B_{0\varphi}+b_\varphi)$$

$$+\rho'(\rho E_1^m - \rho' E_c^m)(B_{0z} + b_z)d\rho'dz' + \int_0^R \rho' D_c^m|_{z'=H}(B_{0\rho} + b_\rho)$$

$$-\rho' D_s^m|_{z'=H}(B_{0\varphi} + b_\varphi)d\rho' - \int_{-H}^H R(B_{0z} + b_z)D_c^m|_{\rho'=R}dz'$$

$$+\int_0^R \rho' D_s^m|_{z'=-H}(B_{0\varphi} + b_\varphi) - \rho' D_c^m|_{z'=-H}(B_{0\rho} + b_\rho)d\rho'] \tag{21}$$

$$A_z = \frac{1}{4\pi}[\int_{-H}^H \int_0^R -\rho'\rho E_s^m(B_{0\rho} + b_\rho) + \rho'(\rho' E_1^m - \rho E_c^m)(B_{0\varphi} + b_\varphi)d\rho'dz'$$

$$+\int_{-H}^H RD_1^m|_{\rho'=R}(B_{0\varphi} + b_\varphi)dz'], \tag{22}$$

where the following abbreviations of azimuthal integrals were used:

$$D_s^m(\rho, \rho', z, z') = \int_0^{2\pi} \frac{\sin\varphi' \sin m\varphi'}{(\rho^2 - 2\rho\rho'\cos\varphi' + \rho'^2 + (z-z')^2)^{\frac{1}{2}}}d\varphi'$$

$$D_c^m(\rho, \rho', z, z') = \int_0^{2\pi} \frac{\cos\varphi' \cos m\varphi'}{(\rho^2 - 2\rho\rho'\cos\varphi' + \rho'^2 + (z-z')^2)^{\frac{1}{2}}}d\varphi'$$

$$D_1^m(\rho, \rho', z, z') = \int_0^{2\pi} \frac{\cos m\varphi'}{(\rho^2 - 2\rho\rho'\cos\varphi' + \rho'^2 + (z-z')^2)^{\frac{1}{2}}}d\varphi'.$$

In our numerical scheme, we typically use equidistant grid points $\rho_i = i \times \Delta r$ and $z_j = j \times \Delta z$ to discretize the intervals $[0, R]$ and $[-H, H]$, respectively (in some applications non-equidistant grid points are also used). The extended trapezoidal rule is applied to approximate all the integrals in Eqs. (14-22). Then we obtain the following matrix equations

$$\begin{pmatrix} b_\rho \\ b_\varphi \\ b_z \end{pmatrix} = \mu\sigma \left[\mathbf{P} \begin{pmatrix} B_{0\rho} + b_\rho \\ B_{0\varphi} + b_\varphi \\ B_{0z} + b_z \end{pmatrix} - \mathbf{Q} \begin{pmatrix} \phi_{s1} \\ \phi_{s2} \\ \phi_{s3} \end{pmatrix} - \lambda\mathbf{R} \begin{pmatrix} A_\rho \\ A_\varphi \\ A_z \end{pmatrix} \right], \tag{23}$$

$$\frac{1}{2}\begin{pmatrix} \phi_{s1} \\ \phi_{s2} \\ \phi_{s3} \end{pmatrix} = \mathbf{S} \begin{pmatrix} B_{0\rho} + b_\rho \\ B_{0\varphi} + b_\varphi \\ B_{0z} + b_z \end{pmatrix} - \lambda\mathbf{T} \begin{pmatrix} A_\rho \\ A_\varphi \\ A_z \end{pmatrix} - \mathbf{U} \begin{pmatrix} \phi_{s1} \\ \phi_{s2} \\ \phi_{s3} \end{pmatrix}, \tag{24}$$

$$\begin{pmatrix} A_\rho \\ A_\varphi \\ A_z \end{pmatrix} = \mathbf{W} \begin{pmatrix} B_{0\rho} + b_\rho \\ B_{0\varphi} + b_\varphi \\ B_{0z} + b_z \end{pmatrix}, \tag{25}$$

9

where the matrix elements of $\mathbf{P}$, $\mathbf{Q}$, $\mathbf{R}$, $\mathbf{S}$, $\mathbf{T}$, $\mathbf{U}$, and $\mathbf{W}$ can be read off from Eqs.(14-22). Combining Eqs.(23-25), we obtain

$$(\mathbf{I} - \mu\sigma\mathbf{E} - \mu\sigma\lambda\mathbf{F})\mathbf{b} = \mu\sigma(\mathbf{E} + \lambda\mathbf{F})\mathbf{B}_0, \qquad (26)$$

where

$$\mathbf{E} = \mathbf{P} - \mathbf{Q} \cdot (\frac{1}{2}\mathbf{I} + \mathbf{U})^{-1} \cdot \mathbf{S} \qquad (27)$$

$$\mathbf{F} = \mathbf{Q} \cdot (\frac{1}{2}\mathbf{I} + \mathbf{U})^{-1} \cdot \mathbf{T} \cdot \mathbf{W} - \mathbf{R} \cdot \mathbf{W} \,. \qquad (28)$$

After solving the algebraic equation system (26), the induced magnetic field $\mathbf{b}$ can be obtained for the magnetic induction process.

For the kinematic dynamo problem, the following generalized eigenvalue problem has to be solved

$$(\mathbf{I} - \mu\sigma\mathbf{E}) \cdot \mathbf{b} = \lambda^*\mathbf{F} \cdot \mathbf{b} \qquad (29)$$

for the given velocity field $\mathbf{u}$, where $\lambda^* = \mu\sigma\lambda$. Note that a quite similar numerical scheme can be established in spherical geometry for the case of axisymmetric dynamo sources.

3   NUMERICAL IMPLEMENTATION AND RESULTS

In this section, the integral equation approach will be applied to various cylindrical dynamo and induction problems of experimental relevance. We start with the problem of the free decay of a magnetic field in a cylinder. Then, a class of Beltrami-like flows will be considered. In all the problems we use the QZ algorithm [27] which is a modification of the QR algorithm for the case of generalized non-hermitian eigenvalue problems.

The integral equation approach is further employed to investigate the induction effect of the VKS experiment. The algebraic equation system is solved by the LU decomposition. The obtained induced magnetic field will be compared with the data measured in experiment.

At the end we deal with the Riga dynamo experiment with its large ratio of height to radius. Due to the large resulting matrices we shift here from direct matrix inversion methods to the generalized inverse iteration method [28].
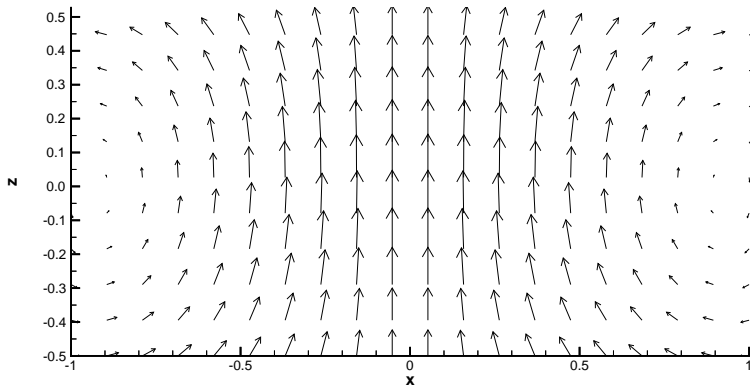
10

Fig. 1. Freely decaying magnetic field in a finite cylinder with $R = 2H = 1$.

3.1 Free field decay in a finite cylinder

The simplest problem to start with is the free decay of a magnetic field in a finite length cylinder. This example was already treated by Iskakov et al. [10]. In Fig. 1 we show the magnetic field lines of the slowest decaying eigenfield, which has the same dipolar structure as in Fig. 8 in [10].

3.2 Beltrami-like flows

In this subsection, we consider a class of flows in finite cylinders which we call "Beltrami-like" flows. Actually, the velocity field $\mathbf{v}(\mathbf{r})$ of Beltrami flows are characterized by the property $\nabla \times \mathbf{v} = \beta \mathbf{v}$. In dynamo theory, there is particular interest in such flows since they are also helicity maximizing. Helicity maximizing flows, in turn, are well known to possess quite small critical R_m, a fact that was utilized, e.g., in the optimization of the Riga dynamo experiment [7]. The actual flow structures that will be treated in this work were proposed by J. Léorat [29], and a certain sub-class of them (with ideally conducting boundary conditions, however) was considered by Wang et al. [30].

We use the notation $s_m^{\pm} t_n$ to characterize flows with m poloidal vortices and n toroidal vortices. The sign $\pm$ indicates that the poloidal flow in the equatorial plane is directed inward $(+)$ or outward $(-)$, respectively. An impression of the topology of the flow structure can be obtained from Fig. 2 where we have also indicated possible propeller or rotating disk configurations to produce such flows.

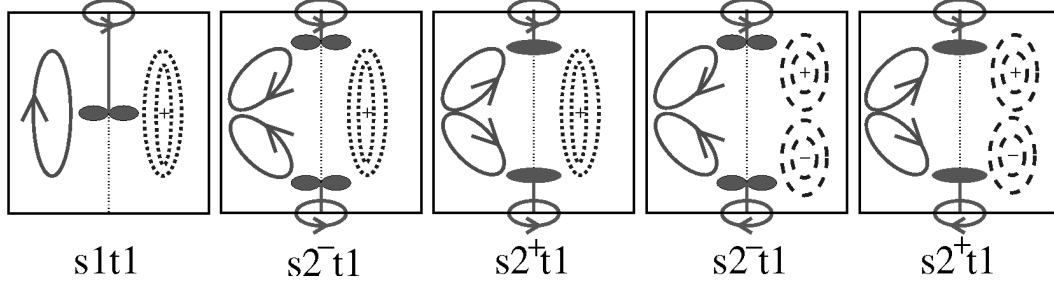The analytical expression of the flows to be considered in this paper are as follows:

11

$$s1t1 \qquad s2^-t1 \qquad s2^+t1 \qquad s2^-t1 \qquad s2^+t1$$

Fig. 2. Illustration of the considered flow topologies $s_m^{\pm} t_n$, and of typical propeller or rotating disk configurations to produce them.

$$v_r(r, z) = c_1 \, J_1(\alpha \, r) \cos(m\pi(z + H)/2H), \tag{30}$$
$$v_\varphi(r, z) = \tau \, J_1(\alpha \, r) \cos(n\pi(z + H)/2H), \tag{31}$$
$$v_z(r, z) = -c_1 \, c_2 \, \alpha/\pi \, J_0(\alpha \, r) \sin(m\pi(z + H)/2H), \tag{32}$$

where $\alpha = 3.8317$ is the first root of the Bessel function J_1. In the following, we will restrict ourselves to $m, n = 1, 2$. $c_1 = 1$ for all $s_m^+ t_n$ flows, $c_1 = -1$ for all $s_m^- t_n$ flows, $c_2 = H/2$ for $s_1 t_1$ flow and for other flows $c_2 = 1$. Again, $2H$ is the height of the cylinder, $z \in [-H, H]$. In the following discussion the height of the cylinder is set to 2 and the radius is fixed to 1. The parameter τ indicates the ratio of toroidal to poloidal flow. We will consider values of τ close to 2 which turned out to be advantageous for dynamo action. Actually, this value $\tau = 2$ is not the value which would correspond to an excact Beltrami flow. This is the reason why we have called the considered flows "Beltrami-like".

In what follows we will use a definition of the magnetic Reynolds number R_m which is based on the maximum of the axial velocity. In order to display the results for the $s_m^{\pm} t_n$ in one common figure we will use the $\pm$ as a sign of R_m according to $R_m = \pm \mu \sigma R |v_z^{max}|$.

For the case without external layer ($w = 0$) we found that only the $s_2^+ t_2$ dynamo is steady, all the others are all oscillatory. However, if an external layer around the finite cylinder is added, even the thickness of the layer is quite small, for example, equal to 0.05, the $s2^- t2$ dynamo becomes steady.

The magnetic field structures for $s_1 t_1$, $s_2^- t_1$, $s_2^+ t_1$, $s_2^- t_2$ and $s_2^+ t_2$ flows are shown, at an azimuthal section at $\varphi = 0$, in Figs. 3, 5, 6, 8 and 9, respectively. In all these cases, an externally added layer with thickness equal to 0.5 has been considered. The variations of growth rates of the magnetic fields with respect to the magnetic Reynolds number for all the flows are depicted in Figs. 4, 7 and 10. From these figures, one can see that the externally added layer has a very strong impact on the onset of dynamo actions. For example, the critical magnetic Reynolds number for the flow $s_2^- t_1$ is approximately equal to 143 in the case without external layer. When an external layer with thickness 0.2 is considered, the critical magnetic Reynolds number reduces to 61. If the thickness of the external layer is increased to 0.5, the critical
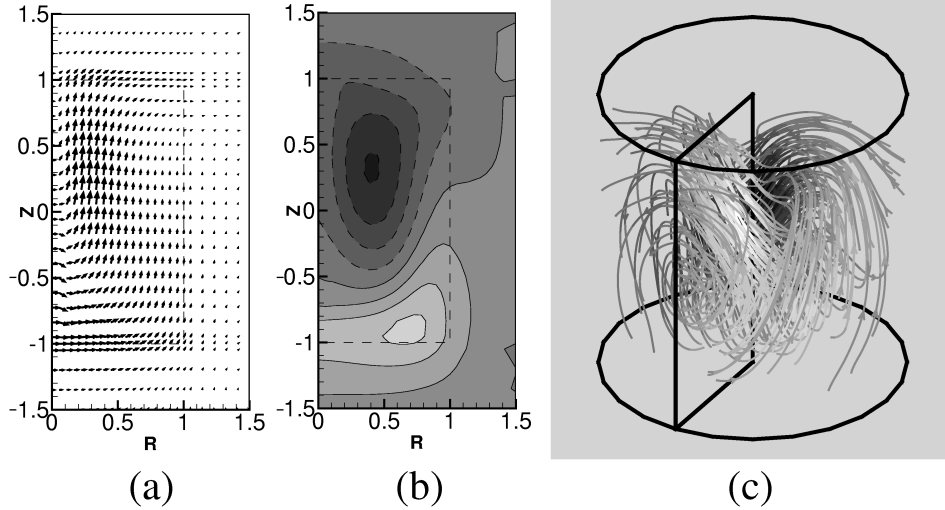
Fig. 3. Magnetic field structure for s_1t_1 flow with $w = 0.5$. (a) Poloidal field component. (b) Contour plot of the toroidal field component. (c) Three dimensional field structure.
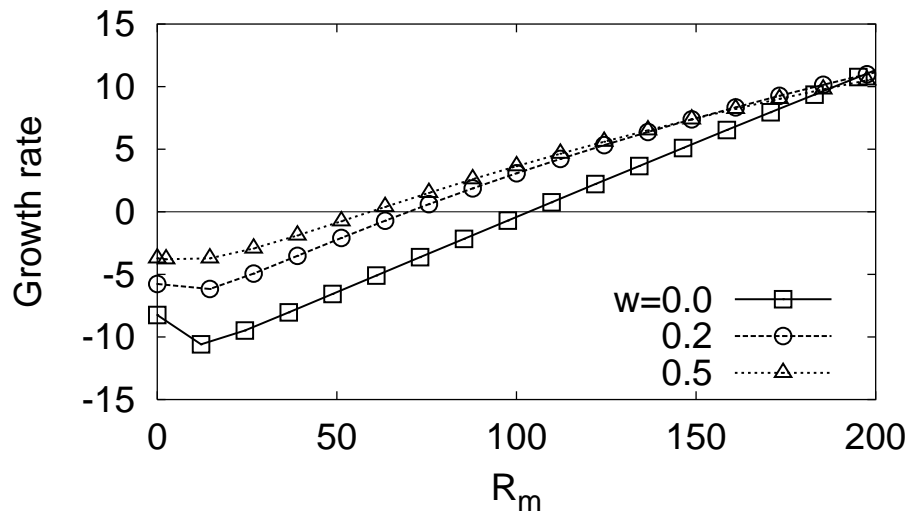

Fig. 4. Growth rates for s_1t_1 flow and the influence of the externally added layers with thickness w.

magnetic Reynolds number further declines to 40. Finally, one can also note that there is a tendency that when the thickness of the external layer becomes larger, the curves of the growth rates become more symmetric with respect to the ordinate axis at $R_m = 0$.

In Fig. 11 we show, for the flow $s_2^+ t_2$ with different widths w of the external layer, the dependence of the critical R_m on the parameter τ which measures the ratio of toroidal to poloidal motion. For $w = 0$ we show, in addition to the results of the integral equation approach, also the results of a finite difference code based on the differential equation approach as it was described in [7] and also used in [19]. In general, we observe a good correspondence of the results
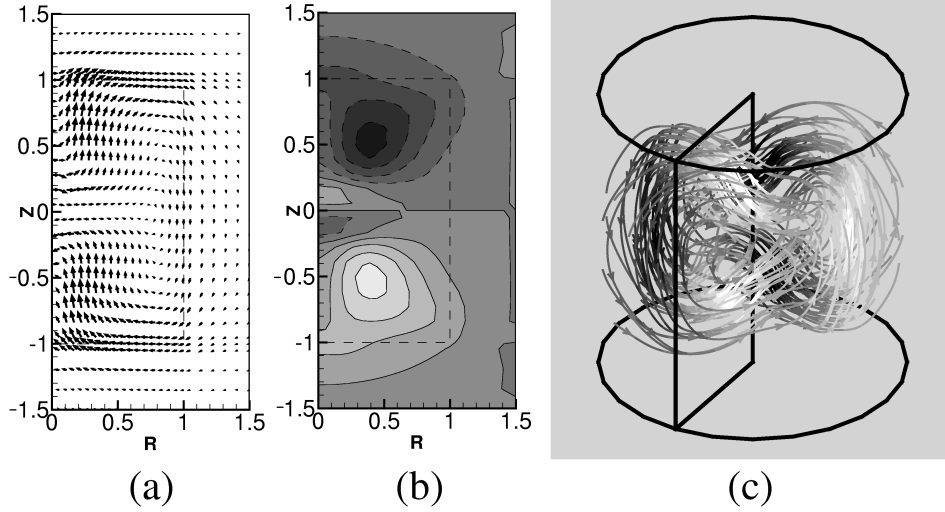
13

(a)   (b)   (c)

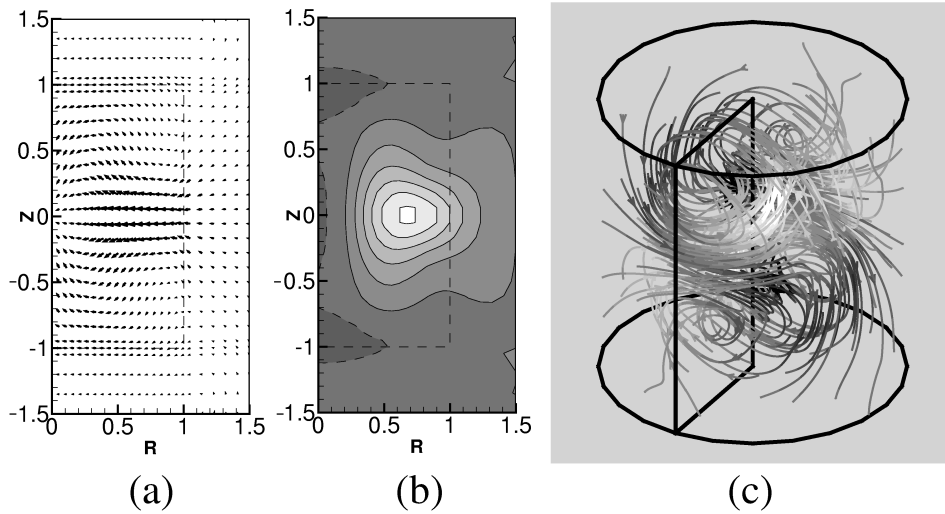Fig. 5. Magnetic field structure for $s_2^- t_1$ flow

(a)   (b)   (c)

Fig. 6. Magnetic field structure for $s_2^+ t_1$ flow.

of both methods which, however, deteriorates slightly for increasing values of τ.

3.3 Induction effects in the VKS Experiment

Since the $s_2^+ t_2$ flows are characterized by a comparatively low critical R_m, much focus was laid on their realization in experimental dynamos. Both the spherical Madison dynamo experiment (MDX) [31,32] and the cylindrical "von Kármán sodium" experiment (VKS) [22,23] are realizations of the $s_2^+ t_2$ flow.

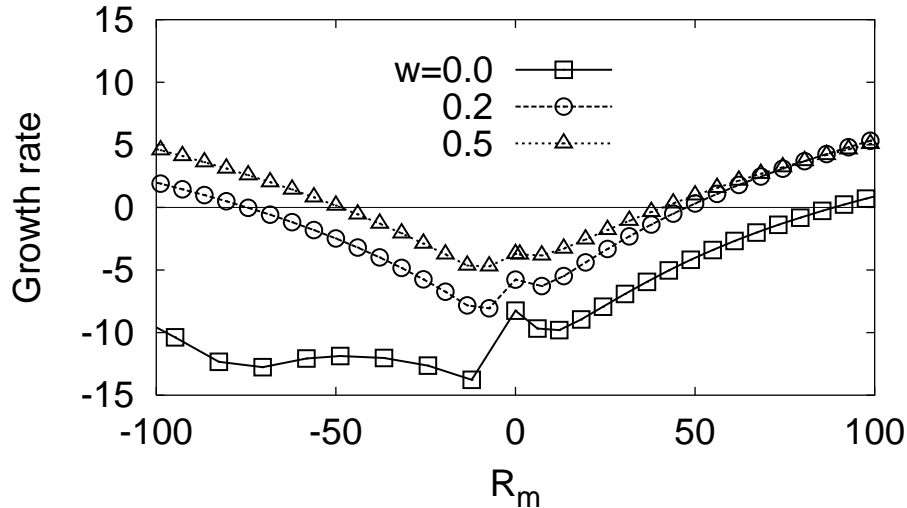Although a recent version (using impellers with a high magnetic permeability

14

Fig. 7. Growth rates for $s_2^{\pm}t_1$ flow and influence of the externally added layers.
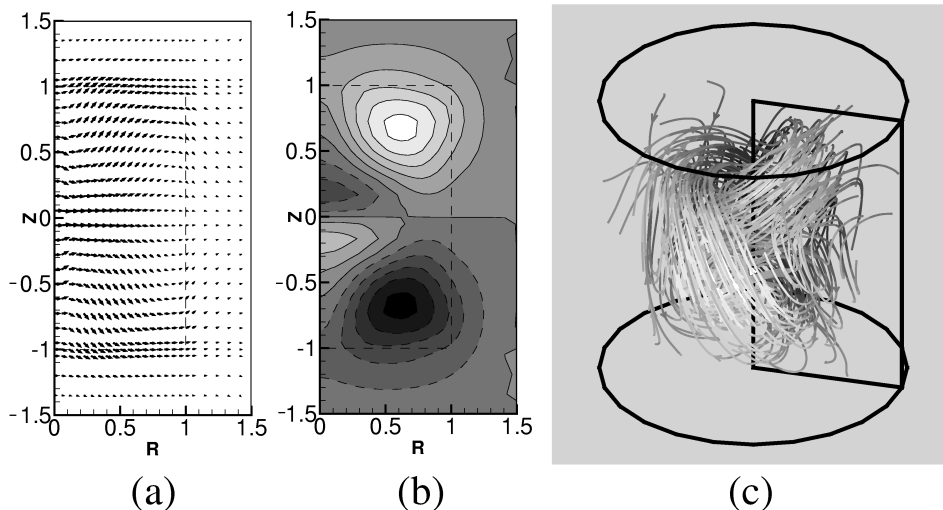

(a) (b) (c)

Fig. 8. Magnetic field structure for $s_2^{-}t_2$ flow

$\mu_{rel} \sim 200$) of the VKS experiment has shown dynamo action [20] and even a kind of polarity reversals [21], the under-performance of the original VKS experiment compared to numerical predictions is still a matter of interest. In [19] we have tried to explain this by the detrimental effect of sodium layers behind the propellers on the dynamo action. The sheer existence of these layers leads already to a significant increase of the critical R_m which becomes dramatic if a realistic rotation therein is taken into account.

Interestingly, in the original VKS experiment, the measured induced magnetic fields, for large R_m, are significantly weaker than the numerically predicted ones. Using our method we will try to figure out if this effect can also be attributed to the existence of lid layers and the flow therein.
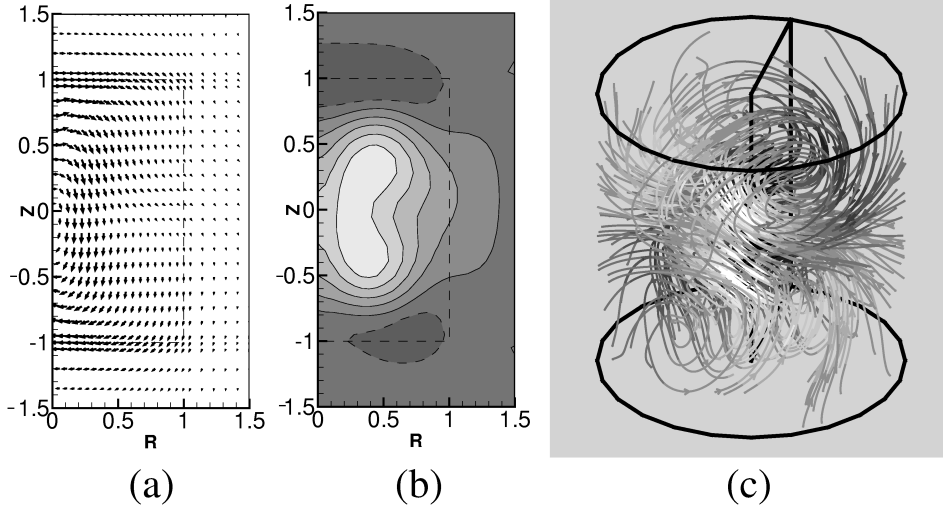
15

(a)   (b)   (c)

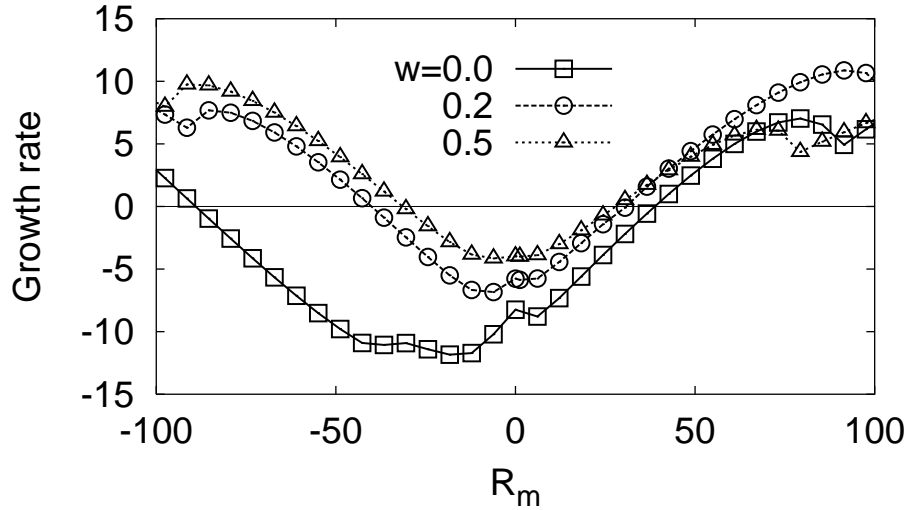Fig. 9. Magnetic field structure for $s_2^+ t_2$ flow.

Fig. 10. Growth rates for $s_2^\pm t_2$ flow and influence of the externally added layers

A rather realistic flow field, resulting from the so-called TM73 propeller[34] (which was identified as a sort of optimal flow field), is considered in our calculation. Some interpolations were necessary to project this flow field onto the grids used in our code. More details on this can be found in [19].

In the original VKS experiment a static external magnetic field was applied in the transverse direction. The induced magnetic field was measured in the direction perpendicular to the externally added magnetic field at the point $r = 0.5$ in the equatorial plane. In the following the induced magnetic fields near the $r = 0.5$ points obtained by our integral equation approach are compared with the measured ones. The influence of a rotating flow in the lid layer on the induced field is investigated. Three kinds of velocity field in the lid layer are considered. The first one is a static lid layer. The second one is that only
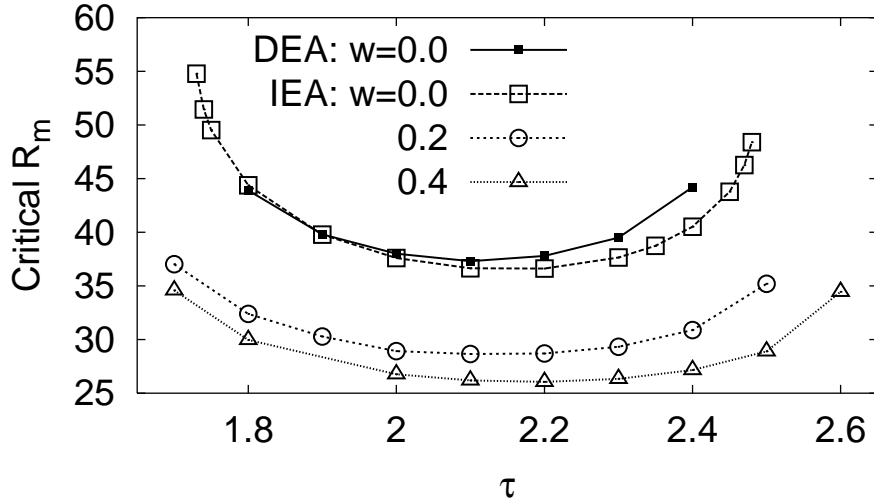
Fig. 11. Critical R_m for the $s_2^+ t_2$ flow in dependence on the toroidal/poloidal ratio τ for different thicknesses w of the surrounding layer. For $w = 0$, we compare the results with the results of a differential equation solver.
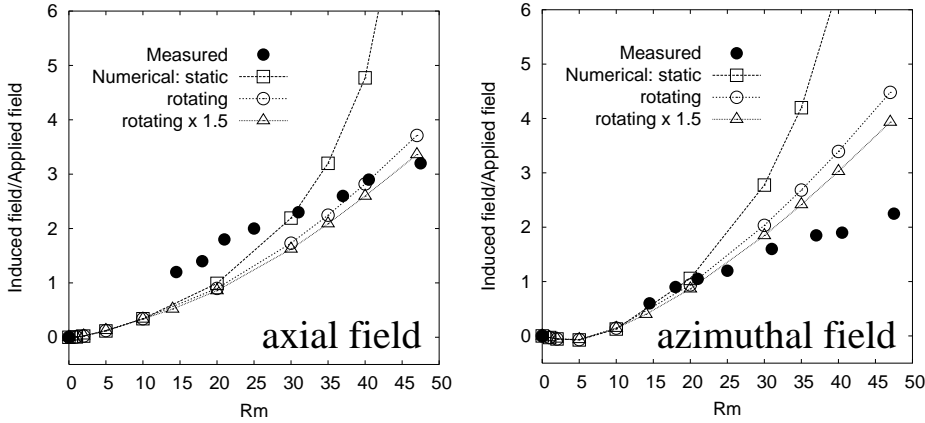

Fig. 12. Ratio of induced axial (left) and azimuthal (right) magnetic field to the applied magnetic field. Experimental results at radius $r = 0.5$ (taken from [35]) and numerical results under the assumptions of different flows in the lid layer. Static lid layer, constant velocity in lid layer, constant velocity in lid layers multiplied by factor 1.5.

a rotation of the lid layer is assumed, but v_φ remains constant in the axial direction, its dependence on the radial variable is the same as on the interface between the lid layer and inner part of the cylinder. The third one has only one difference from the second case in that the magnitude of v_φ is increased by a factor 1.5 which comes closer to the velocity of the impeller. For these three cases, the numerical axial induced fields around the point $r = 0.5$ and the experimental result at $r = 0.5$ on the equatorial plane are shown in the left part of Fig. 12 for different magnetic Reynolds numbers. The right panel of Fig. 12 displays the azimuthal induced magnetic fields. From these figures one can see that the third case shows a best agreement with the experimental one.
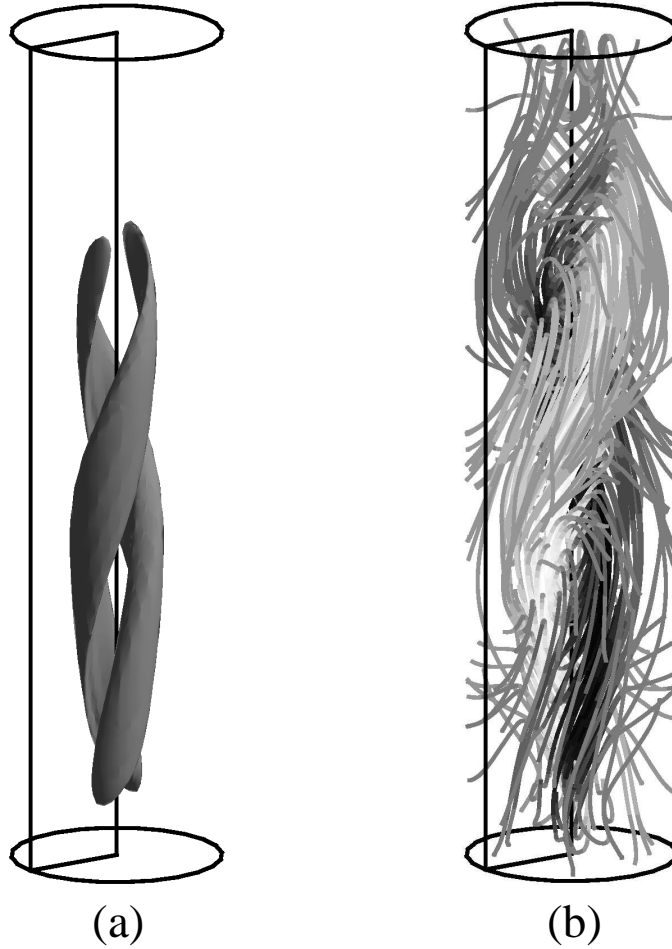
17

(a)   (b)

Fig. 13. Simulated magnetic field structure of the eigenmode of the Riga dynamo experiment. (a) Isosurface plot of the magnetic field energy. The isosurface corresponds to 25 per cent of the maximum magnetic energy. (b) Magnetic field lines.

A good agreement of the axial magnetic field with the experimental result has been achieved for the second and third cases. But for the azimuthal magnetic field, when the magnetic Reynolds number is larger than 30, there is still a gap between the numerical results and the experimental ones.

Nevertheless it is quite likely that it is indeed the existence of lid layers and some azimuthal flow therein which is responsible for the unexpected under-performance of the original VKS dynamo experiment.

3.4 Riga experiment

In this subsection, the integral equation approach is used to re-simulate the kinematic regime of the Riga dynamo experiment. This experiment has been optimized and analyzed extensively within the differential equation approach
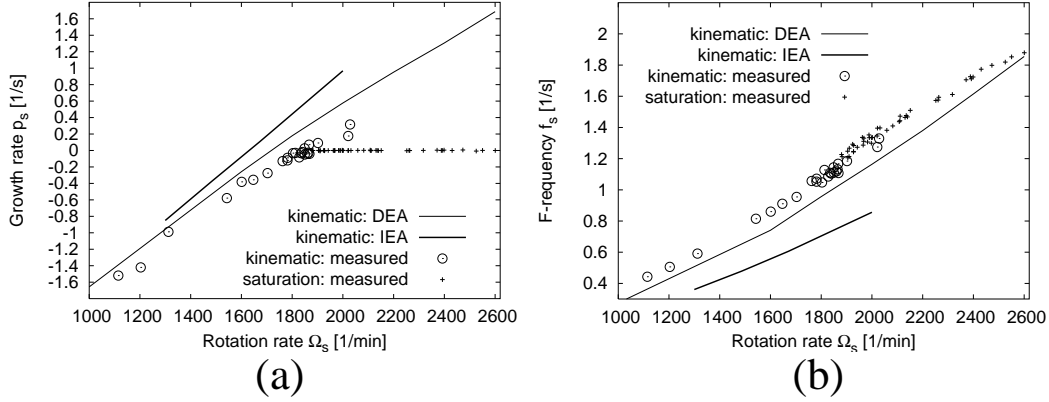
Fig. 14. Comparison of the IEA and DEA results for the Riga dynamo experiment, together with experimental results. (a) Growth rate. (b) Frequency.

(DEA) by means of a finite difference solver [7]. The values of the velocity field on the grids used in our code are obtained by interpolating the experimental velocity field measured in a water-dummy experiment. The influence of less conducting stainless steel walls has not been taken into account.

The computations have been carried out on a 100×20 grid in z- and r-direction. The structure of the magnetic eigenfield is illustrated in Fig. 13. Figure 13a shows the isosurface of the magnetic field energy (this time at 25 percent of the maximum value). In Fig. 13b the magnetic eigenfield lines are depicted. Basically the structure is the same as that resulting from the differential equation approach [26] with a 401×64 grid in z- and r-direction.

The dependence of the growth rate and frequency of the eigenmode of the Riga dynamo experiment on the rotation rate is shown in Fig. 14a and Fig.14b, respectively. The comparison with the DEA results shows that the slopes of the curves are in good agreement. However, we see that the limited grid resolution in the IEA leads to significant shifts in the order of 5 percent towards lower rotation rates for the growth rate and of 10 per cent towards higher rotation rate for the frequency. Hence, it could be said that the Riga dynamo experiment marks a margin of reasonable applicability of the IEA with its need to invert large matrices which are fully occupied.

4   CONCLUDING REMARKS

In the present paper, the integral equation approach to kinematic dynamos has been applied to non-spherical geometries. The method was examined by its application to the free field decay. The comparison of the obtained results with other methods shows a good agreement. The integral equation approach was extended to investigate induction effects of the VKS experiment. The obtained

induced magnetic field shows a satisfactory agreement with the experimental result when the effect of the lid layers and a certain azimuthal flow therein are taken into account. Finally, it was applied to simulate the Riga dynamo experiment.

It can be concluded that the integral equation approach is robust and reliable and can be used for practical purposes, although limits of its applicability are seen for the Riga dynamo experiment with its large ratio of length to radius.

References

[1] G. Rüdiger and R. Hollerbach. The magnetic universe, Wiley-VCH, Weinheim, 2004.

[2] A. Gailitis, O. Lielausis, E. Platacis, G. Gerbeth, and F. Stefani. Laboratory experiments on hydromagnetic dynamos, Rev. Mod. Phys. 74 (2002) 973-990.

[3] A. Brandenburg, A. Nordlund, R.F. Stein, and U. Torkelsson, Dynamo-generated turbulence and large scale magnetic fields in a Keplerian shear flow, Astrophys. J. 446 (1995) 741-754.

[4] S. Kenjereš and K. Hanjalić, Numerical simulation of a turbulent magnetic dynamo, Phys. Rev. Lett. 98 (2007) 104501.

[5] K.-H. Rädler, E. Apstein, M. Rheinhardt, and M. Schüler. The Karlsruhe dynamo experiment - a mean-field approach, Stud. Geophys. Geod. 42 (1998) 224-231.

[6] K.-H. Rädler, M. Rheinhardt, E. Apstein, and H. Fuchs. On the mean-field theory of the Karsruhe dynamo experiment, Nonl. Proc. Geophys. 9 (2002) 171-178.

[7] F. Stefani, G. Gerbeth and A. Gailitis, Velocity profile optimization for the Riga dynamo experiment, in: A. Alemany, Ph. Marty, and J.-P. Thibault (Eds.), Transfer Phenomena in Magnetohydrodynamics and Electroconducting Flows, Kluwer, Dordrecht, 1999, pp. 31-44.

[8] J.-L. Guermond, J. Léorat, and C. Nore, A new Finite Element Method for magneto-dynamical problems: two-dimensional results, Eur. J. Mech. B/Fluids 22 (2003) 555-579.

[9] R. Laguerre, C. Nore, J. L'eorat and J.-L. Guermond, Effects of conductivity jumps in the enveloppe of a kinematic dynamo flow, Comptes Rendus Mecanique 334 (2006) 593-598.

[10] A.B. Iskakov, S. Descombes, and E. Dormy, An integro-differential formulation for magnetic induction in bounded domains: boundary element-finite volume method, J. Comp. Phys. 197 (2004) 540-554.

[11] A.B. Iskakov and E. Dormy, On magnetic boundary conditions for non-spectral dynamo simulations, Geophys. Astrophys. Fluid Dyn. 99 (2005) 481-492.

[12] A. Gailitis, Self-excitation of a magnetic field by a pair of annular vortices, Magnetohydrodynamics 6 No. 1 (1970) 14-17.

[13] A. Gailitis and Ya. Freibergs, Self-excitation of a magnetic field by a pair of annular eddies, Magnetohydrodynamics 10 No. 1 (1974) 26-30.

[14] Ya. Freibergs, Optimization of the shape of the toroidal model of an MHD dynamo, Magnetohydrodynamics 11 No. 3 (1975) 269-272.

[15] W. Dobler and K.-H. Rädler, An integral equation approach to kinematic dynamo models, Geophys. Astrophys. Fluid Dyn. 89 (1998) 45-74.

[16] F. Stefani, G. Gerbeth, and K.-H. Rädler, Steady dynamos in finite domains: an integral equation approach, Astron. Nachr. 321 (2000) 65-73.

[17] M. Xu, F. Stefani, and G. Gerbeth, The integral equation method for a steady kinematic dynamo problem, J. Comp. Phys. 196 (2004) 102-125.

[18] M. Xu, F. Stefani, and G. Gerbeth, Integral equation approach to time-dependent kinematic dynamos in finite domains, Phys. Rev. E 70 (2004) 056305.

[19] F. Stefani, M. Xu, G. Gerbeth, F. Ravelet, A. Chiffaudel, F. Daviaud, J. Léorat, Ambivalent effects of added layers on steady kinematic dynamos in cylindrical geometry: application to the VKS experiment, Eur. J. Mech./B Fluids 25 (2006) 894-908.

[20] R. Monchaux et al., Generation of a magnetic field by dynamo action in a turbulent flow of liquid sodium, Phys. Rev. Lett. 98 (2007) Art. No. 044502.

[21] M. Berhanu et al., Magnetic field reversals in an experimental turbulent dynamo, Europhys. Lett. 77 (2007) 59001.

[22] M. Bourgoin et al., Magnetohydrodynamics measurements in the von Kármán sodium experiment, Phys. Fluids 14 (2002) 3046-3058.

[23] F. Pétrélis et al., Nonlinear magnetic induction by helical motion in a liquid sodium turbulent flow, Phys. Rev. Lett. 90 (2003) 174501.

[24] A. Gailitis et al., Detection of a flow induced magnetic field eigenmode in the Riga dynamo facility, Phys. Rev. Lett. 84 (2000) 4365-4368.

[25] A. Gailitis et al.. Magnetic field saturation in the Riga dynamo experiment, Phys. Rev. Lett. 86 (2001) 3024-3027.

[26] A. Gailitis, O. Lielausis, E. Platacis, G. Gerbeth, and F. Stefani, Riga dynamo experiment and its theoretical background, Phys. Plasmas 11 (2004) 2838-2843.

[27] C. Moler and G. W. Stewart, An algorithm for generalized matrix eigenvalue problems, SIAM J. Numer. Anal. 10 (1973) 241-256.

[28] D.J. Ivers and C.G. Phillips, A vector spherical harmonic spectral code for linearised magnetodydrodynamics, ANZIAM J. 44 (E) (2003) C423-C442.

[29] J. Léorat, personal communication

[30] Z. Wang, V.I. Pariev, C.W. Barnes, D.C. Barnes, Laminar plasma dynamos, Phys. Plasmas 9 (2002) 1491-1494.

[31] E.J. Spence, M.D. Nornberg, C.M. Jacobson, R.D. Kendrick, and C.B. Forest, Observation of a turbulence-induced large scale magnetic field, Phys. Rev. Lett. 96 (2006) 055002.

[32] M.D. Nornberg, E.J. Spence, R.D. Kendrick, C.M. Jacobson, and C.B. Forest, Intermittent magnetic field excitation by a turbulent flow of liquid sodium, Phys. Rev. Lett. 97 (2006) 044503.

[33] L. Marié, C. Normand, and F. Daviaud, Galerkin analysis of kinematic dynamos in the von Kármán geometry, Phys. Fluids 18 (2004) 017102.

[34] F. Ravelet, A. Chiffaudel, F. Daviaud, J. Léorat, Towards an experimental von Kármán dynamo: numerical studies for an optimized design, Phys. Fluids 17 (2005) 117104.

[35] F.Ravelet, Bifurcations globales hydrodynamiques et magnétohydrodynamiques dans un écoulement de von Kármán turbulent, Ph.D. Thesis, CEA Saclay, (2005).